

General Disclaimer

One or more of the Following Statements may affect this Document

- This document has been reproduced from the best copy furnished by the organizational source. It is being released in the interest of making available as much information as possible.
- This document may contain data, which exceeds the sheet parameters. It was furnished in this condition by the organizational source and is the best copy available.
- This document may contain tone-on-tone or color graphs, charts and/or pictures, which have been reproduced in black and white.
- This document is paginated as submitted by the original source.
- Portions of this document are not fully legible due to the historical nature of some of the material. However, it is the best reproduction available from the original submission.

"Made available under NASA sponsorship
in the interest of early and wide dis-
semination of Earth Resources Survey
Program information and without liability
for any use made thereof."

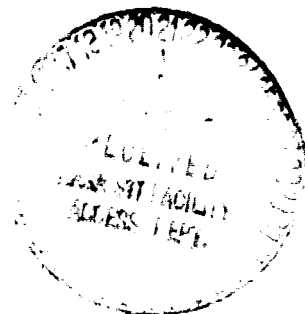
183-10388
CR-172930

TO Harold Oseroff
Code 902
NASA Goddard Spaceflight Center
Greenbelt, MD 20771

FROM Jeff Dozier
Department of Geography
University of California
Santa Barbara, CA 93106

CC Contracting Officer, NASA/GSFC
Publications Section, NASA/GSFC
Patent Counsel, NASA/GSFC
James Foster, NASA/GSFC
Carlena Leufroy, ONR, Pasadena

Quarterly Progress Report, Contract No. NAS5-27463
Landsat-D Investigations in Snow Hydrology



(E83-10388) LANDSAT-D INVESTIGATIONS IN
SNOW HYDROLOGY Quarterly Progress Report
(California Univ.) 23 p HC A02/MF A01

N83-32141

CSCL 08H

Unclass

G3/43 00388

Results to Date

We have now received two Landsat-4 TM tapes (7 bands) within our study area in the southern Sierra Nevada (path 41, row 35, 10 December 1982, and path 42, row 34, 13 January 1983). During the reporting period we have worked on registration of the TM data to digital topographic data, on comparison of TM, MSS and NOAA meteorological satellite data for snowcover mapping, and on radiative transfer models for atmospheric correction.

These investigations are described in more detail below.

**Account ledgers for June are incomplete.

Presentations by Principal Investigator

1. April 20, 1983, *Snow Reflectance from the Thematic Mapper*, Institute of Remote Sensing, Academia Sinica, Beijing, China.
2. April 20, 1983, *Slope, Horizon, and Drainage Basin Information from Digital Terrain Models*, Institute of Remote Sensing, Academia Sinica, Beijing, China.
3. April 22, 1983, *Remote Sensing and Snow Hydrology*, Institute of Remote Sensing, Academia Sinica, Beijing, China.
4. April 22, 1983, *Image Processing Software at University of California, Santa Barbara*, Institute of Remote Sensing, Academia Sinica, Beijing, China.
5. April 26, 1983, *Emissivity and Infrared Brightness Temperature of Snow*, Institute of Remote Sensing, Academia Sinica, Beijing, China.
6. May 1, 1983, *Snow Hydrology Research and Remote Sensing*, Tien Shan Glaciological Station, Urümqi River Basin, China.
7. May 4, 1983, *Snow Hydrology Research and Remote Sensing*, Xinjiang Institute of Geography, Urümqi, China.
8. May 5, 1983, *Fundamental Radiometric Properties*, Xinjiang Institute of Geography, Urümqi, China.
9. May 5, 1983, *Emissivity of Snow*, Xinjiang Institute of Geography, Urümqi, China.
10. May 7, 1983, *Remote Sensing and the Snow Surface Radiation Budget*, Institute of Glaciology and Cryopedology, Academia Sinica, Lanzhou, China.
11. May 7, 1983, *Emissivity of Snow*, Institute of Glaciology and Cryopedology, Academia Sinica, Lanzhou, China.
12. May 8, 1983, *Remote Sensing in the U.S.*, Gansu Province Institute of Remote Sensing, Lanzhou, China.
13. June 6, 1983, *Remote Sensing of the Snow Surface Radiation Budget*, California Space Institute, Scripps Institute of Oceanography, University of California, San Diego.

Detailed Descriptions of Investigations

1. EFFECT OF SPATIAL RESOLUTION ON THE ACCURACY OF MAPPING SNOW COVERED AREA

1.1. Synopsis

Satellite data from three sensors, Landsat-4 TM and MSS, and NOAA-7 AVHRR, will be used to map snow covered area (SCA) over selected basins to determine the error associated with using coarser spatial resolution. This information is needed to quantify the information lost when high resolution data are not available and to determine the minimum resolution requirements for basins of different sizes. The effect of a discontinuous snowcover within a basin will also be evaluated. This effort will improve our ability to make quantitative comparisons of surface measurements made with different satellite instruments

Satellite remote sensing has become increasingly important to hydrologists because it provides information on the spatial distribution of parameters of hydrologic importance. In snow and ice studies, remote sensing has been used to improve the monitoring of existing conditions and has been incorporated into several runoff forecasting and management systems. *Rango* [1979] presents a detailed review of research in this area through 1978, and the *Snow and Ice*, chapter of the *5th Pecora Symposium* [Deutsch et al., 1981] has descriptions of several applications currently implemented or being tested.

The most common operational use of remote sensing in snow studies is to monitor the areal extent of the snowcover [Barnes and Bouley, 1974; Foster and Rango, 1975; McGinnis et al., 1975; Rango and Itten, 1976; Rango and Salomonson, 1976]. These efforts led other investigators to conclude that satellite derived estimates of snow covered area [SCA] could be used to improve forecasting of snowmelt runoff [Hannaford, 1977; Rango et al., 1977; Rango, 1978; Rango et al., 1979; Brown et al., 1980]. Martinac [1975] and Rango and Martinac [1979] carried this a step further in their model by including satellite derived measurements of SCA as an index to melt. Satellites can also be viewed as space-borne radiometers. Techniques have been developed to use these data to measure or estimate snow surface characteristics that are necessary for calculation of the surface radiation budget [Dozier, 1980a, 1981, 1982, 1983; Dozier et al., 1980, 1981; Dozier and Frew, 1981; Dozier and Warren, 1982; Frampton and Marks, 1980; Marks, 1982]. While these efforts go beyond mapping SCA, any use of satellite data for snow hydrology begins with the mapping of the snow cover distribution over the surface. To determine the spatial accuracy of any type of satellite data, we begin with the estimate of SCA.

The efforts cited above have all been influenced by the availability, cost, and characteristics of data from satellite instruments that are currently operational. Operational applications have usually been limited to the measurement of SCA from uncorrected photographic products using manual photo interpretation techniques. Digital snow mapping techniques, while faster and less subjective, have been limited to specific experiments because of processing difficulties and the high cost of satellite data in digital form. For these reasons no effort has been made to assess the relative spatial accuracy of utilizing satellite data in different forms or from different instruments to estimate SCA. The purpose of this investigation is to conduct an experiment to determine the advantages and disadvantages of using data from different satellite instruments. From this we will evaluate the effect of basin size and shape, and discontinuous snowcover on the accuracy of our estimate of SCA for several different types of satellite data.

1.2. Satellite Data

Environmental satellite data are available in a variety of forms that are useful to snow hydrologists. For our investigations on the effect of resolution we will use data from the Landsat Thematic Mapper (TM) and Multispectral Spectral Scanner (MSS), and from the NOAA Advanced Very High Resolution Radiometer (AVHRR). These are multichannel instruments that are frequently used to map SCA over basins from 10 km^2 to $10,000 \text{ km}^2$. Table 1 presents a comparison of these instruments.

Table 1					
Characteristics of TM, MSS, and AVHRR Satellite Data (spectral, spatial, temporal, and economic)					
Landsat-4 Thematic Mapper (TM)					
band	wavelengths (50% ampl., μm)		nominal pixel size	overpass interval	digital data cost
1	.452	- .518	28.5 m	16 days	\$2500
2	.529	- .610			
3	.624	- .693			
4	.776	- .905			
5	1.568	- 1.784			
7	2.097	- 2.347			
6	10.422	- 11.661	114 m		
Landsat-4 Multispectral Scanner (MSS)					
1	.497	- .607	57 m	16 days	\$650
2	.603	- .697			
3	.704	- .814			
4	.809	- 1.036			
NOAA-7 Advanced Very High Resolution Radiometer (AVHRR)					
1	.56	- .72	1.1 km	12 hrs.	\$75
2	.71	- .98			
3	3.53	- 3.94			
4	10.32	- 11.36			
5	11.45	- 12.42			
Digital data costs are approximate for the TM as they are not yet available to the public. For this investigation we have the TM data in hand. Digital data costs for the AVHRR reflect our costs to travel to Scripps SSOF, use of the facility, and return to UCSB. It is assumed that at least four data sets are acquired per trip.					

We have acquired TM and MSS data for the southern Sierra Nevada from NASA Goddard for December 10, 1982. We have received an additional TM data set for the central Sierra Nevada for January 13, 1983. We will acquire AVHRR data from the Scripps Satellite Oceanographic Facility (SSOF) for the same overpass dates, and we hope to acquire one additional MSS data set to correspond to the January TM overpass.

1.3. The Experiment

By acquiring data from three different environmental satellites over the same area on the same date, we have the uncommon opportunity to compare the spatial accuracy associated with using each type to estimate SCA. We plan to answer the following fundamental questions:

- * For basins of several different sizes and shapes, how much difference is there in our estimate of SCA when using TM, MSS, and AVHRR data?
- * Under what conditions of basin size, and snow cover distribution will coarse resolution AVHRR data provide adequate information on SCA?
- * How can occasional inputs from TM or MSS data be used to improve estimates of SCA that are regularly made with AVHRR data?

These questions are important because while high resolution TM data are undoubtedly more accurate, they are expensive, difficult to acquire with reasonable regularity, and beyond the digital processing capability of most researchers. MSS data are the most commonly used satellite data, but they also have poor temporal resolution, and are expensive. AVHRR data are inexpensive, and the satellite has frequent overpasses, but the coarse spatial resolution makes the data difficult to use in small basins, or under conditions of sparse or patchy snowcovers.

The research is divided logically into two parts. The first step is to calibrate and register the three satellite data sets to a standard reference. This is by far the most difficult part of the work, and will take the most time and effort. The development of the QDIPS image processing system at the Computer Systems Laboratory, University of California, Santa Barbara, makes this registration possible. The second involves the selection of test basins of varying sizes and snowcover distributions for the mapping of SCA using each type of satellite data. Each of these is described in detail below.

1.3.1. *Calibrating and Registering Satellite Data Sets to a Reference Grid*

Before the satellite data can be analyzed, the following processing is required:

- * Radiometric correction: Pixel values must be converted to the appropriate physical units (surface exitance or brightness temperature).
- * Geometric correction: The satellite imagery must be geometrically transformed so that it will overlay our digital terrain database.

The flow of processing is as follows:

1.3.2. *Radiometric correction*

TM, MSS, and AVHRR shortwave data are converted to surface exitances using a simple linear transform whose multiplicative and additive terms are assumed to be constant [Lauritson et al., 1979; Engel, 1980; Clark and Dasgupta, 1983]. Since these coefficients may change over an image frame time, the radiometric correction must be performed before any geometric corrections alter the original time-space relationships within the image.

1.3.3. *Geometric correction*

Our terrain database is constructed from USGS digital elevation data. The data are supplied in geodetic coordinates (latitude, longitude). During the process of extracting a region of interest, we transform the data to the Universal Transverse Mercator (UTM) projection. We have adopted the UTM projection as our geographic reference since it maintains almost constant scale over areas of the sizes in which we are interested, and is readily indexed in common units of measurement (meters). Accurate, computationally efficient formulas are available to convert between UTM and geodetic (latitude and longitude) coordinates [Dozier, 1980b]. The spatial resolution of the

individual terrain data sets ("terrain grids") will be resampled to 28.5 meters, corresponding to the highest satellite resolution (TM) to be used in this investigation.

Our problem is therefore to transform the TM, MSS, and AVHRR data into the UTM coordinate system of the terrain grids, at the selected spatial resolution. For TM and MSS data, the standard digital products supplied by NASA in the Space Oblique Mercator (SOM) projection. The SOM projection has been mathematically defined [Snyder, 1981], but computer code implementing the conversions between SOM and geodetic coordinates is not currently available. We will therefore have to develop programs for mapping from SOM into UTM. Scale changes will be accommodated by resampling. Any misregistration will be corrected by polynomial fitting of ground control points (GCPs). Experience of other users of TM and MSS data leads us to believe that any such residual misregistrations are largely translational in nature, and therefore easily corrected by a few GCPs [David Pitts, NASA Johnson Space Flight Center, personal communication].

AVHRR data as obtained from the Satellite Oceanographic Facility at the Scripps Institute of Oceanography have had no geometric corrections performed. The general problem of georeferencing satellite imagery requires precise determination of the position (altitude and nadir point) and attitude (yaw, pitch, and roll) of the satellite, together with a model of the spatial resolution of the sensor system. We are currently implementing systems to predict satellite positions using *a posteriori* orbital element data, and to build a satellite attitude vector from telemetered yaw, pitch, and roll data. These models are tuned by least-squares adjustment of their coefficients using control points with known geodetic locations. This procedure will be used to determine the mapping between AVHRR image coordinates and UTM coordinates, using control points selected from pseudo-image displays of the terrain grid.

The end product of the geometric correction process will be TM, MSS, and AVHRR data sets registered to digital terrain models and resampled to 28.5 meter resolution. Since this resampling represents an interpolation of up to 10x (in the AVHRR case), we will investigate whether high-order resampling techniques affect SCA determination in any systematic fashion (we suspect that the effect will be negligible).

1.3.4. Mapping Snowcovered Area

Several basins that are partially snowcovered and vary in size from 25 to 2500 km^2 will be selected. To find partially snowcovered basins that are small we will select areas near the Owens valley where small basins have a larger elevation change. Estimates of SCA for each basin will be made using each satellite data type. Basins will be digitally isolated using a procedure developed by Marks *et al.*, [1983] and mapping of SCA will be done with existing software in the QDIPS system. In each case, the TM data will be used as the *reference standard* to determine the "best" estimate of SCA as well as the spatial contiguity of the snowcover. Results from the MSS and AVHRR data will then be compared to this standard.

In addition to the digital mapping of SCA for each test basin, James Foster, an experienced photo interpreter from NASA Goddard Space Flight Center will manually map SCA for each satellite data type. We will use this information to evaluate the relative accuracy of manual over automated snow mapping techniques for satellite data of different spatial resolutions.

1.4. Significance of this Research

The immediate importance would be in the improved utility of satellite data for mapping SCA. A reduced dependence on more expensive high resolution data from the MSS or TM sensors would save costs, and implementation of automated digital techniques would improve the efficiency of state and federal water management programs. In the long run, the improved understanding of satellite data and their potentials and limitations, should provide broad benefits to both hydrology and remote sensing.

2. ATMOSPHERIC RADIATIVE TRANSFER MODEL ACCOUNTING FOR BOTH THE ZENITH AND AZIMUTH VARIATIONS IN THE RADIATIVE FIELD

2.1. Synopsis

In remote sensing, the signature obtained by the satellite sensor is related to radiance, which is a function of elevation, location, and viewing angle, in addition to the astronomic and atmospheric conditions.

In order to infer the radiometric properties of the medium underlying the atmosphere from remotely sensed data, atmospheric correction of the satellite data is necessary. In remote sensing for oceanography, quick atmospheric correction algorithms have been developed [Gordon, 1978; Gordon and Clark, 1980] and successfully applied to the quantitative assessment of chlorophyll concentration in Southern California [Smith and Wilson, 1981]. In these algorithms, the known spectral optical properties of water are used to determine the aerosol path radiance at wavelength 670 nm, where the subsurface upwelling radiance is negligible, and then to estimate the aerosol path radiance at other wavelengths. However, in other wavelengths, or for other types of surfaces besides water, the application of these algorithms may be limited, because of the different optical properties. Therefore, some general atmospheric correction algorithms are required.

In our project, a different approach, which invokes an atmospheric radiative transfer model accounting for both the zenith and azimuth variation in the radiative field, is taken. The model deals with a plane parallel structured atmosphere, which is composed of different layers with each assumed to be homogeneous in composition and to have linear-in- τ temperature profile. Moreover, the multiple scattering between such an atmosphere and the underlying medium (say, water, snow, or soil), which may have both the zenith and azimuth variation in radiative behavior, is taken into consideration.

This approach is an extension of an azimuthally integrated atmospheric radiative transfer model developed by Wiscombe [1981], which is based on the results of earlier researchers [Grant and Hunt, 1969] and his own investigations [Wiscombe, 1976a, 1976b]. The additional parameter on azimuthal variation is handled by adding a new azimuth dimension into the computation space. In order to save computation time, the Fourier transform is performed over the azimuth domain. Then the resulting Fourier coefficients with different order stand for the original vector and work in a parallel manner, so that the array sizes for each order of coefficient in the computation remain the same as for the azimuthally integrated case. The final radiance are obtained by inverse Fourier transformation from the Fourier coefficients of those quantities, which are the results derived from the procedures similar to what is used for calculating the azimuthally integrated radiance.

The inputs of such a model are some astronomic and atmospheric parameters for each layer (or level), and the surface radiative property. Those parameters or properties can be obtained either by some model or by measurements. The astronomical parameters are earth-sun distance and solar flux at the top of the atmosphere, and the atmospheric parameters include pressure temperature, chemical composition of the air molecules, and the composition and size of the aerosol, water droplets, and ice crystals. The outputs of the model are the monochromatic radiance and irradiance of at each level. By integration, the total radiance and irradiance can be obtained.

The potential application of this model in the atmospheric correction of remote sensing include several aspects. For example: after calculating the upward radiance at the top of the atmosphere for an atmosphere with black surface beneath it, and then by removing this value from the radiance measured at the top of the atmosphere, one can get the modified radiance which accounts for the contribution of upward radiance at the surface level.

Also, this model can mimic the angular radiative field for a plane parallel layered atmosphere - earth system, in which the earth surface property is homogeneous from location to location. For low frequency spatial variation, this model may also offer good approximation. For more complicated cases with high frequency spatial variation, this model may approximate the average radiance over an area with certain size. The departure from the average may be used to derive more detailed information of the surface.

Besides, this model will be useful to assess the other atmospheric correction algorithms, in which some aspects of the interaction between radiation and medium may be omitted. Because this model considers all the aspects of the interaction between photon and medium for a plane parallel structured absorbing and scattering system, if we apply the other algorithms on such a system, the departure of the results of the two models will give an indication of the performance of the algorithm to be assessed.

2.2. Review of Radiation Model

Once the atmosphere is subdivided into many plane parallel homogeneous layers according to some atmosphere model or some measurement data, the basic inherent radiative properties, such as the total optical depth, the single scattering albedo, and the phase function can be derived for each layer by Rayleigh scattering, Mie scattering, line absorption and continuum absorption theories.

Based on those basic properties, the reflection and transmission functions, and the solar and thermal source function for each layer can be determined, and finally, the radiances at desired levels can also be calculated, using the radiative transfer theory.

In the following sections, we will deal with a K -layer atmosphere plus underlying medium model.

2.2.1. Radiative Transfer Equation

The radiative transfer equation for a plane parallel medium is given by [Chandrasekhar, 1960]

$$\mu \frac{dL(\tau, \mu, \varphi)}{d\tau} + L(\tau, \mu, \varphi) = J(\tau, \mu, \varphi).$$

τ is optical depth, and $L(\tau, \mu, \varphi)$ is the radiance at level τ along direction μ, φ (where μ is cosine of zenith angle and φ is azimuth angle). The source function is given by

$$J(\tau, \mu, \varphi) = \frac{\omega}{4\pi} \int_0^{2\pi} \int_{-1}^1 P(\tau, \mu, \varphi; \mu', \varphi') L(\tau, \mu', \varphi') d\mu' d\varphi' + Q(\tau, \mu, \varphi)$$

The last term represents an internal source. The internal source term in this case is similar to that for the azimuthally averaged case [Wiscombe, 1976].

$$Q(\tau, \mu, \varphi) = Q_t(\tau, \mu, \varphi) + Q_d(\tau, \mu, \varphi) + Q_s(\tau, \mu, \varphi)$$

The thermal source is

$$Q_t(\tau, \mu, \varphi) = (1 - \omega) B(T(\tau))$$

$B(T(\tau))$ is the Planck function at temperature T , where T is a function of optical depth. The direct source and specular "pseudo-source" arising from the diffuse - direct splitting of the radiance are

$$Q_d(\tau, \mu, \varphi) = \frac{\omega E_0}{4\pi} P(\tau, \mu, \varphi; \mu_0, \varphi_0) e^{-\tau/\mu_0}$$

and

$$Q_s(\tau, \mu, \varphi) = \frac{\bar{\omega} E_0}{4\pi} \rho_s(\mu_0) P(\tau, \mu, \varphi; -\mu_0, \varphi_0) e^{-2(\tau_I - \tau)/\mu_0}$$

Here μ_0 is the cosine of the solar zenith angle, E_0 is the solar irradiance incident on the top of the atmosphere (normal to the beam), and ρ_s is the directional specular reflectivity at the surface beneath the atmosphere.

2.2.2. Interaction Principle

One way to attack this integro - differential equation is using the "interaction principle" [Grant and Hunt, 1969] which, specified to a layer bounded by τ_I and τ_J across which $\bar{\omega}$ and phase function P are constant, assumes the discrete form

$$L^+(\tau_J) = r(\tau_I, \tau_J) L^-(\tau_J) + t(\tau_J, \tau_I) L^+(\tau_I) + \Sigma^+(\tau_I, \tau_J)$$

$$L^-(\tau_I) = r(\tau_J, \tau_I) L^+(\tau_I) + t(\tau_I, \tau_J) L^-(\tau_J) + \Sigma^-(\tau_I, \tau_J)$$

Radiance $L^\pm(\tau)$, ($\tau = \tau_I, \tau_J$) is a vector of $m \times n$ elements on a discrete angular space composed of m zenith and n azimuth angles

$$L^\pm(\tau) = \begin{bmatrix} L(\tau, \pm\mu_1, \varphi_1) \\ L(\tau, \pm\mu_1, \varphi_2) \\ \dots \\ L(\tau, \pm\mu_m, \varphi_n) \end{bmatrix}$$

$0 < \mu_1 < \dots < \mu_m \leq 1$ are a set of quadrature points for (0,1). $0 \leq \varphi_1 < \dots < \varphi_n < 2\pi$ are equally spaced points in the interval $0-2\pi$. $r(\tau_I, \tau_J)$ and $t(\tau_I, \tau_J)$ are reflection and transmission matrices. $\Sigma^\pm(0, \tau)$ are internal source vectors. The r , t and Σ for each of the homogeneous single layer can be derived by some initialization scheme and the doubling method.

2.2.3. Initialization

In a recent letter, Wiscombe suggests that the Infinitesimal Generator Initialization (IGI) is best [Grant and Hunt, 1969]. It produces the $r(\Delta\tau)$, $t(\Delta\tau)$, and $\Sigma^\pm(\Delta\tau)$ for an optically very thin starting layer with optical depth $\Delta\tau$. After initialization, the $r(\tau_I, \tau_{I+1})$, $t(\tau_I, \tau_{I+1})$, and $\Sigma^\pm(\tau_I, \tau_{I+1})$ for the entire homogeneous layer bounded by levels I and $I+1$ can be derived.

The IGI claims

$$r(\Delta\tau) = \frac{\bar{\omega} \Delta\varphi \Delta\tau}{4\pi} M^{-1} P^{+-} C$$

$$t(\Delta\tau) = I - \Delta\tau M^{-1} I + \frac{\bar{\omega} \Delta\varphi \Delta\tau}{4\pi} M^{-1} P^{++} C$$

where I, M, C are matrices of size $mn \times mn$. M^{-1} is the inverse of M . I is the identity matrix, M and C are diagonal matrices,

$$M = [\mu_i \delta_{ij} \delta_{kl}]$$

$$C = [c_i \delta_{ij} \delta_{kl}]$$

and

$$P^{++} = [P(\mu_i, \varphi_k; \pm\mu_j, \varphi_k)]$$

where $1 \leq i \leq m$, $1 \leq j \leq m$, $1 \leq k \leq n$, and $1 \leq l \leq n$, and μ_i 's are the cosines of zenith angles derived by some quadrature rule (say, Gaussian quadrature rule), and the c_i 's are the associated weights, and δ_{ij} is delta function defined as $\delta_{ij} = 1$ if $i=j$, otherwise $\delta_{ij} = 0$.

The source vectors for different source need to be handle separately. The [G] gives the general relation between source term Q 's and the source vectors for the initial layer

$$\Sigma^{\pm}(\Delta\tau) = M^{-1} \int_{\tau_1}^{\tau_1 + \Delta\tau} \begin{bmatrix} Q(\tau, \pm\mu_1, \varphi_1) \\ Q(\tau, \pm\mu_1, \varphi_2) \\ \dots \\ Q(\tau, \pm\mu_n, \varphi_n) \end{bmatrix} d\tau$$

The solar source vector for the initial thin layer is

$$\Sigma_s^{\pm}(\delta\tau) = \frac{\mathfrak{S} E_0}{4\pi} \frac{\mu_0}{|\mu|} e^{-\tau/\mu_0} (1 - e^{-\delta\tau/\mu_0}) P(\pm\mu, \varphi_k; \mu_0, \varphi_0)$$

and the thermal source term

$$\Sigma_f^{\pm}(\Delta\tau) = (1 - \mathfrak{S}) \frac{B \Delta\tau}{|\mu|}$$

However, the thermal source vectors for the entire homogeneous layer with linear-in-tau temperature profile within it can be derived in a quite simple fashion without directly using $\Sigma_f^{\pm}(\Delta\tau)$.

2.2.4. Adding and Doubling Method

By applying the interaction principle to two adjacent layers, the reflection and transmission matrices and the source vectors for the combined layer can be derived if the corresponding quantities are known for each of these two layers [Grant and Hunt, 1969].

Consider two adjacent layers bounded by planes x, y, z . By the interaction principle, we have

$$\begin{aligned} L^+(y) &= t(y, x) L^+(x) + r(x, y) L^-(y) + \Sigma^+(x, y) \\ L^-(x) &= r(x, y) L^+(x) + t(x, y) L^-(y) + \Sigma^-(x, y) \\ L^+(z) &= t(z, y) L^+(y) + r(y, z) L^-(z) + \Sigma^+(y, z) \\ L^-(y) &= r(y, z) L^+(y) + t(y, z) L^-(z) + \Sigma^-(y, z) \end{aligned}$$

Since x, y, z are entirely arbitrary, we can use the interaction principle and write

$$\begin{aligned} L^+(z) &= t(z, x) L^+(x) + r(x, z) L^-(z) + \Sigma^+(x, z) \\ L^-(x) &= r(x, z) L^+(x) + t(x, z) L^-(z) + \Sigma^-(x, z) \end{aligned}$$

These equations can be obtained by eliminating $L^+(y)$ and $L^-(y)$ from those before. Then the following relations hold

$$\begin{aligned} r(z, x) &= r(y, x) + t(x, y) [I - r(z, y) r(x, y)]^{-1} r(z, y) t(y, x) \\ r(x, z) &= r(y, z) + t(z, y) [I - r(x, y) r(z, y)]^{-1} r(x, y) t(y, z) \\ t(z, x) &= t(z, y) [I - r(x, y) r(z, y)]^{-1} t(y, x) \\ t(x, z) &= t(x, y) [I - r(z, y) r(x, y)]^{-1} t(y, z) \\ \Sigma^+(z, x) &= t(z, y) [I - r(x, y) r(z, y)]^{-1} r(x, y) \Sigma^-(y, z) + \\ &+ t(z, y) [I - r(x, y) r(z, y)]^{-1} \Sigma^+(y, x) + \Sigma^+(x, y) \\ \Sigma^-(x, z) &= t(x, y) [I - r(z, y) r(x, y)]^{-1} r(z, y) \Sigma^+(y, x) + \\ &+ t(x, y) [I - r(z, y) r(x, y)]^{-1} \Sigma^-(y, z) + \Sigma^-(x, y) \end{aligned}$$

These are the formulae for the so called "adding" method. If the two layers are

identical, the method is called "doubling." If the initial layer is chosen such that

$$\Delta\tau = (\tau_{I+1} - \tau_I) / 2^N$$

where N is a integer, and $(\tau_{I+1} - \tau_I)$ is the optical depth of the $I+1$ th layer in the multi-layer system, then the reflection and transmission matrices and source vectors for such a homogeneous thick layer can be built up quickly by "doubling" N times:

$$t_{n+1} = t_n (I - \tau_n \tau_n)^{-1} t_n$$

$$\tau_{n+1} = \tau_n + t_n (I - \tau_n \tau_n)^{-1} \tau_n t_n$$

$$\tau_n = \tau(2^n \Delta\tau), t_n = t(2^n \Delta\tau), \text{ and } 0 \leq n \leq N$$

Since neither of the internal sources, including the solar and thermal sources, are constant with optical depth, nor the changes of them with optical depth the same, they need to be treated separately. For the solar source, the doubling scheme takes a special form:

$$\Sigma_{d,n+1}^+ = t_n \tau_n (e_n \tau_n \Sigma_{d,n}^- + \Sigma_{d,n}^+) + e_n \Sigma_{d,n}^+$$

$$\Sigma_{d,n+1}^- = t_n (\tau_n \Sigma_{d,n}^+ + e_n \Sigma_{d,n}^-) + \Sigma_{d,n}^-$$

For initial layer, $n=0$, $e_0 = e^{-\Delta\tau/\mu_0}$, and $e_{n+1} = e_n^2$.

For a layer with linear-in- τ temperature profile, the doubling method gives the final resulting thermal source vectors as [Wiscombe, 1976]:

$$\Sigma_{t,N}^+ = \frac{1}{2}(B_0 + B_N) Y_N \pm B' Z_N$$

where

$$B_0 = B[T(\tau_I)]$$

$$B_N = B[T(\tau_{I+1})]$$

$$B' = [(B_N - B_0) / (\tau_{I+1} - \tau_I)]$$

Z_N can be obtained recursively:

$$Z_{n+1} = Z_n + g_n Y_n + (t_n \Gamma_n - t_n \Gamma_n \tau_n) (Z_n - g_n Y_n)$$

$$g_n = 2^{n-1} \Delta\tau$$

$$Y_{n+1} = (t_n \Gamma_n \tau_n + t_n \tau_n + I) Y_n$$

with the initial values $Z_0=0$, $g_0=\frac{1}{2}\Delta\tau$ and $Y_0=(1-\omega)\Delta\tau M^{-1}U$. U is a vector of ones, and $\Gamma=(I - \tau_n \tau_n)^{-1}$

Then the total source vectors for the entire homogeneous layer are the sum of all the different types of internal sources.

$$\Sigma_{\hat{t}} = \Sigma_{d,N}^+ + \Sigma_{t,N}^+ + \dots$$

2.2.5. Calculation of the Internal Radiance

Having known the reflection and transmission matrices, and the source vectors for each layer in the multi-layer system, we can build the internal radiance field in the atmosphere by the adding method. Using formulae of the interaction principle, we have a set of simultaneous equations:

$$L^+(\tau_{I+1}) = t(\tau_{I+1}, \tau_I) L^+(\tau_I) + \tau(\tau_I, \tau_{I+1}) L^-(\tau_{I+1}) + \Sigma^+(\tau_I, \tau_{I+1})$$

$$L^-(\tau_I) = \tau(\tau_{I+1}, \tau_I) L^+(\tau_I) + t(\tau_I, \tau_{I+1}) L^-(\tau_{I+1}) + \Sigma^-(\tau_I, \tau_{I+1})$$

for $0 \leq I < K$, where K is the total number of layers in the system, and $\tau_0=0$ and τ_K is total optical depth of the atmosphere. In addition, two sets of boundary conditions need to be satisfied:

$$L^+(\tau_0) = L^+(0)$$

is the top boundary condition.

$$L^-(\tau_K) = R_G L^+(\tau_K) + \epsilon B(T_G) + \frac{\mu_0 E_0}{\pi} e^{-\tau_K/\mu_0} f\tau(\mu_0)$$

is the bottom boundary condition. R_G is the surface diffuse reflection matrix, $f\tau(\mu_0)$ is the BRDF (bidirectional reflectance-distribution functions) vector for the incident beam, and T_G is the temperature of the surface.

It is convenient to solve this set of equations in the following recursive manner.

1. Compute recursively the intermediate partial interactive quantities from top to bottom for each layer (or level).

This is so called forward pass. In this stage, the calculation starts at the top layer, then goes down, and for each layer only the contribution made by the internal source of the current layer and by the radiation coming from above, and the interaction between the current layer and the layers above are taken into account. There are six quantities calculated. They represent the partial upward and downward radiance fields, and incident-from beneath reflection and transmission operator, respectively. The precise physical meanings of these quantities can be understood from the following recursive formulae and the initial values for them.

$$V_I^- = [I - \tau(\tau_{I+1}, \tau_I) RE_{I-1}]^{-1} [\Sigma^{-1}(\tau_I, \tau_{I+1}) + \tau(\tau_{I+1}, \tau_I) V_{I-1}^-]$$

$$V_I^+ = V_{I-1}^+ + RE_{I-1} V_I^-$$

$$V_I^* = \Sigma^+(\tau_I, \tau_{I+1}) + t(\tau_{I+1}, \tau_I) V_I^+$$

$$H_I = [I - \tau(\tau_{I+1}, \tau_I) RE_{I-1}]^{-1} t(\tau_I, \tau_{I+1})$$

$$G_I = RE_{I-1} H_I$$

$$RE_I = \tau(\tau_0, \tau_{I+1}) = \tau(\tau_I, \tau_{I+1}) + t(\tau_{I+1}, \tau_I) G_I$$

where $I=0, \dots, K-1$ and the initial values for them are given by

$$V_0^- = \Sigma^-(\tau_0, \tau_1) + \tau(\tau_1, \tau_0) L^+(\tau_0)$$

$$V_0^+ = L^+(\tau_0)$$

$$V_0^* = \Sigma^+(\tau_0, \tau_1) + t(\tau_1, \tau_0) L^+(\tau_0)$$

$$RE_0 = \tau(\tau_0, \tau_1)$$

$$G_0 = 0$$

$$H_0 = t(\tau_0, \tau_1)$$

2. Calculate the radiance at the atmosphere - earth interface.

From the forward pass we have calculated the total contribution of the internal sources and the radiation coming from the top boundary to the downward radiance at the surface level, which is V_{K-1}^- . Using the interaction principle again, we can come up with the final result for the downward radiance at the earth surface.

$$L^+(\tau_K) = [I - RE_{K-1} R_G]^{-1} [V_{K-1}^- + RE_{K-1} (\frac{\mu_0 E_0}{\pi} e^{-\tau_K/\mu_0} f\tau(\mu_0) + \epsilon B(T_G))]$$

The upward radiance at this level can be obtained from the lower boundary condition.

3. Compute recursively the downward and upward radiances from bottom to top. This is so called backward pass.

$$L^+(\tau_I) = V_I^+ + G_I L^-(\tau_{I+1})$$

$$L^-(\tau_I) = V_I^- + H_I L^-(\tau_{I+1})$$

If only the upward radiance at the top of the atmosphere is needed, an alternative procedure can be taken. First, calculate $\tau(x,z)$, $\tau(z,x)$, $t(x,z)$, $t(z,x)$, and $\Sigma^+(x,z)$ successively for the combined layer, each time adding one more layer. Finally, obtain the corresponding quantities for the entire atmosphere.

Then, calculate the upward radiance using

$$L^-(\tau_0) = [\tau(\tau_K, \tau_0) + t(\tau_0, \tau_K) R_G (I - \tau(\tau_0, \tau_K) R_G)^{-1} t(\tau_K, \tau_0)] L^+(\tau_0) +$$

$$\Sigma^-(\tau_0, \tau_K) + t(\tau_0, \tau_K) R_G (I - \tau(\tau_0, \tau_K) R_G)^{-1} \times$$

$$[\Sigma^+(\tau_0, \tau_K) + \tau(\tau_0, \tau_K) \{ \varepsilon B(T_G) + \frac{\mu_0 E_0}{\pi} e^{-\tau_K \mu_0} f\tau(\mu_0) \}]]$$

2.5. Comments

There are several advantages with this model.

1. It considers all aspects of the radiation - medium interaction, including multiple scattering occurring within the atmosphere and between the atmosphere and the underlying medium. The complete consideration of all the aspects in multiple scattering is especially important when the surface has a high reflectance.

2. For surfaces with moderate area size, the algorithm can be used to model the radiance field above it. The modeling accuracy will be good as long as the plane parallel configuration is valid for the situation.

3. This algorithm can also be used to calculate the averaged atmospheric correction amount. When this amount is removed from the remotely sensed data, the resulting radiance values will be good indication of the local surface variation.

4. The algorithm will also be useful for removing cloud interference, as long as the clouds are not opaque in the wavelength concerned.

5. Multiple sources, including thermal source, direct solar beam source, and possibly even specular pseudo source, are taken into account.

6. If the upward radiances at the top of the atmosphere are measured systematically at a set of viewing angles, then the angular radiation field at the surface level can be inferred by inversion.

The disadvantages of this algorithm include the relatively high computation time consumption and relatively large number of input parameters.

3. SOLVING THE ATMOSPHERIC CORRECTION PROBLEM FOR AN INHOMOGENEOUS SURFACE USING A MONTE CARLO METHOD

3.1. Introduction

In remote sensing, Landsat satellites look at the earth at near nadir position and with a very narrow range of viewing angles. Therefore, by fair approximation for our present atmospheric correction algorithm, Landsat looks straight downward at the earth surface.

According to the interaction principle [Grant and Hunt, 1969], the upwelling radiance for a layered structure atmosphere at the height of the satellite can be expressed.

$$L^-(\tau_0) = \tau(\tau_g, \tau_0) L^+(\tau_0) + t(\tau_0, \tau_g) L^-(\tau_g) + \Sigma^-(\tau_0, \tau_g)$$

$\tau_0=0$ is the optical depth at the satellite location, and τ_g is the optical depth at the

ground level. The layer concerned is bounded by the levels at τ_0 and τ_g . $\tau(\tau_g, \tau_0)$ is the reflection matrix of the atmosphere of the layer of atmosphere when the incident light $L^+(\tau_0)$ comes from the top of the layer, $t(\tau_0, \tau_g)$ is the transmission matrix when the incident light $L^-(\tau_g)$ comes from the bottom of the layer, and $\Sigma^-(\tau_0, \tau_g)$ is the contribution of the source within the layer to the upwelling radiance at the satellite level τ_0 .

Note that $L^+(\tau_0)$, $L^-(\tau_g)$, and $\Sigma^-(\tau_0, \tau_g)$ are vectors describing the angular distribution of the radiance, while $\tau(\tau_g, \tau_0)$ and $t(\tau_0, \tau_g)$ are square matrices of corresponding size. Also, note that the incident radiances at boundaries are independent of location by the above formula.

For a given atmosphere, the terms $\tau(\tau_g, \tau_0) L^+(\tau_0)$ and $\Sigma^-(\tau_0, \tau_g)$ can be calculated from an atmospheric radiative transfer model accounting for both zenith and azimuth dependence in a absorbing and scattering layered atmosphere.

The element of $L^-(\tau_0)$ at the nadir viewing angle, denoted as $L^-(\tau_0, \vartheta_v, \varphi_v)$, can be obtained by the satellite measurement. The main concern in remote sensing is to get the quantity $L^-(\tau_g, \vartheta_v, \varphi_v)$, which is an element of $L^-(\tau_g)$ and where ϑ_v and φ_v are the zenith and azimuth angles of the viewing direction of the satellite. For an optically thin atmosphere, the term $L^-(\tau_g, \vartheta_v, \varphi_v)$ is the leading one contributing to the signature $L^-(\tau_0, \vartheta_v, \varphi_v)$. If the pattern of the surface radiance is known or a Lambertian property is assumed, the surface upwelling radiance can be derived given the satellite measurement and the atmospheric profile, using a layered atmospheric radiative transfer model.

However, for most remote sensing, the situation is more complicated, since the upwelling radiance at the earth surface is not independent of location. We can still consider the atmosphere as a layered medium, and within each layer homogeneity can be assumed. In this case, the terms corresponding to $\tau(\tau_g, \tau_0) L^+(\tau_0)$ and $\Sigma^-(\tau_0, \tau_g)$ are still independent of location and remain the same as for a homogeneous surface. Therefore, these two terms can be calculated from the layered radiative transfer model assuming the underlying surface is black and non-emitting. The only problem is that the contribution of the surface upwelling radiance to the upwelling radiance detected by the satellite sensor cannot be simply obtained from the term $t(\tau_0, \tau_g) L^-(\tau_g)$, because $L^-(\tau_g)$ is now location dependent and the corresponding transmission function is also different from the term $t(\tau_0, \tau_g)$ which is related to the integration of the contribution of ground to the radiance at the satellite level over an infinite homogeneous surface area.

Because we are dealing with 2-dimensional surface, we can express the satellite measurement by the following equation:

$$L^-(\tau_0, \vartheta_v, \varphi_v, \xi, \eta) = L_{atm}^-(\tau_0, \vartheta_v, \varphi_v) + \Delta L^-(\tau_0, \vartheta_v, \varphi_v, \xi, \eta) \\ + L^-(\tau_g, \vartheta_v, \varphi_v, x, y) e^{-(\tau_g - \tau_0)/\mu}$$

$\mu = \cos \vartheta_v$ and x, y are the coordinates for the ground position for the measured pixel, and ξ, η are the horizontal coordinates at the satellite level. The first term at the right hand side is the element of $L_{atm}^-(\tau_0)$ at viewing angle (ϑ_v, φ_v) , and the latter is obtained from the layered structure atmospheric radiative transfer model.

$$L_{atm}^-(\tau_0) = \tau(\tau_g, \tau_0) L^+(\tau_0) + \Sigma^-(\tau_0, \tau_g)$$

If we can estimate $\Delta L^-(\tau_0, \vartheta_v, \varphi_v, \xi, \eta)$, then we can obtain $L^-(\tau_g, \vartheta_v, \varphi_v, \xi, \eta)$ using remote sensing measurement and the layered atmospheric model. The Monte Carlo method is one of the suitable candidates for this purpose.

3.2. Monte Carlo Approach

Only the transmission problem is treated, because the reflection and source problem can be solved by the previous model. For a system composed of a layered atmosphere and an underlying inhomogeneous surface, a combination of the azimuth dependent radiative transfer model for the L_{atm}^- term and the Monte Carlo method for transmission of surface upwelling radiance through the atmosphere layer can give a complete expression of the satellite measured radiance.

The proposed model is based on the fact that the contribution of the surface upwelling radiance to the signature of a certain pixel is made by not only the ground element corresponding to the pixel concerned, but also the surrounding area as well. By the reciprocity principle, the pattern of the contribution made by the ground area can be mimicked by a reverse process, a process in which a beam of photons impinges at a given point at the top of the layer and finally some of them get to the surface and make a spread pattern the so called "point-spread" function. In other words, if we can find the point-spread function for a beam impinging on a given atmosphere as a function of incident angle, we can obtain the quantitative expression for the pattern of the contribution of surface upwelling radiance to the satellite measurement. This relation can be written as the following formula:

$$t(\tau_0, \xi, \eta, \vartheta_v, \varphi_v; \tau_g, x, y, \vartheta, \varphi) = t(\tau_g, x, y, \vartheta, \varphi; \tau_0, \xi, \eta, \vartheta_v, \varphi_v)$$

This is the basis of the present algorithm. where t is

$$t(\tau_1, x_1, y_1, \vartheta_1, \varphi_1; \tau_2, x_2, y_2, \vartheta_2, \varphi_2) = \frac{\Delta L(\tau_1, x_1, y_1, \vartheta_1, \varphi_1; \tau_2, x_2, y_2, \vartheta_2, \varphi_2)}{L(\tau_2, x_2, y_2, \vartheta_2, \varphi_2) \cos \vartheta_2 d\omega_2 dA_2}$$

ΔL is the increment of radiance at location (τ_1, x_1, y_1) and in the direction (ϑ_1, φ_1) contributed by the radiant flux at location (τ_2, x_2, y_2) in the direction (ϑ_2, φ_2) .

Note that for this process, the conservation of photons does not hold because some of the incident photons may be absorbed and some of them may get out of the layer through the upper boundary. In either case, the photons are lost and have nothing to do with the transmission point-spread function. Besides, in this configuration, we need not consider the emission problem because the previous adding model has taken care of that process already, and this makes our Monte Carlo method relatively simple.

We need to determine the point-spread function using the Monte Carlo method. Several conditions are given:

1. The beam of photon impinges at the top of the layer of atmosphere concerned.
2. The atmosphere has layered structure and the profiles, including molecular absorption and scattering, Mie scattering components, and temperature, are known.
3. For each sublayer, homogeneity is assumed with the scattering and absorption properties assumed to be the average value derived from the given profile.
4. The relation between optical depth and height should be derived from the atmospheric profile, and be used throughout this algorithm, since this knowledge is crucial for calculating the horizontal position at which the photon gets out of the atmosphere.

The essence of the Monte Carlo method is that the scattering and absorption of the photon can be statistically simulated by a sequence of photons randomly colliding with the medium particles before they finally get absorbed or escape from the medium concerned. Each scattering or absorption is a random event of collision. However, the general trend is governed by some statistical rule according to some probability function of the processes.

In order to mimic this random process, we need some quantities based on some statistical rule. These are the distance traveled by the photon between two random

collision events, the direction of each traveling path, and the chance for the photon to be absorbed upon collision. Also, we need to keep track of position of the photon in three-dimensional space in order to know whether the photon is in the atmosphere, in which sublayer the photon is, and how far it is from the original horizontal position.

The following sections give the mathematical expressions of these events and quantities. Similar descriptions can be found in some representative papers [Cashwell and Everett, 1959; House and Avery, 1969; Pearce, 1977].

3.2.1. Free Path Length

The distance traveled by a photon between collisions is called the free path length. When it is measured in the same manner as the optical depth, it is dimensionless and is called optical distance. The probability density function of the occurrence of noncollision for an optical distance l is

$$p(l) = e^{-l}$$

The probability that no collision occurs in the range of optical distance from 0 to l is

$$r_1 = \int_0^l p(l') dl' = 1 - e^{-l}$$

This equation sets up a unique relation between a random number r_1 ($0.0 \leq r_1 \leq 1.0$) and an optical distance l , and l can be solved explicitly as

$$l = -\ln(1 - r_1) = |\ln(1 - r_1)|$$

Therefore, the distance between scatterings for each path of each photon can be determined according to a random number r_1 generated in some manner.

3.2.2. Chance of Absorption

The single scattering albedo ω of the current sublayer gives the probability $1 - \omega$ that the photon is absorbed upon collision. Conceptually, we can use the idea of photon bundle instead of single photon. Suppose initially a photon bundle impinges into the atmospheric slab. After collision, only a fraction of the photon bundle keeps going and a portion is absorbed. For each collision, the current fraction is multiplied with the single scattering albedo of the current sublayer to get the fraction of the photon bundle continuing. Such a process is repeated until the remaining portion of the photon gets out of the slab or is less than some threshold.

3.2.3. Direction of Scattering

For each scattering event, two independent angular variables can be obtained from random processes, the scattering angle Θ and the azimuth angle Φ which is measured in the plane perpendicular to the original travel direction ϑ_1, ϕ_1 .

The scattering angle Θ is determined in the following way:

define

$$P(\Theta) = \int_0^\Theta p(\Theta') \sin \Theta' d\Theta'$$

Θ' is a dummy variable, $p(\Theta')$ is the phase function for scattering angle Θ' for the current scattering sublayer. Because the integration of $p(\Theta')$ over the range from 0 to π is 2, we need to multiply the quantity expressed by a factor of 0.5 to normalize it. Then we can relate such a quantity to a random number r_2 generated for the random scattering process to determine the scattering angle Θ .

$$\frac{1}{2} P(\Theta) = r_2$$

The angle ϕ is within the range from 0 to 2π , therefore

$$\phi = 2\pi \tau_3$$

where τ_3 is another random number. Both τ_2 and τ_3 are within the range from 0 to 1.

Knowing the original travel direction ϑ_1, φ_1 , and the scattering angle and azimuth θ and ϕ , the travel direction for the next path, ϑ_2, φ_2 , can be determined from

$$\begin{aligned} \cos\vartheta_2 &= \cos\vartheta_1 \cos\theta - \sin\vartheta_1 \sin\theta \cos\phi \\ \tan\varphi_2 &= \frac{\cos\vartheta_1 \sin\varphi_1 \sin\theta \cos\phi + \cos\varphi_1 \sin\theta \sin\phi + \sin\vartheta_1 \sin\varphi_1 \cos\theta}{\cos\vartheta_1 \cos\varphi_1 \sin\theta \cos\phi - \sin\varphi_1 \sin\theta \sin\phi + \sin\vartheta_1 \cos\varphi_1 \cos\theta} \end{aligned}$$

These relations can be derived using the formulae for 3-dimensional axis rotation.

3.2.4. Distance of Penetration of Photon in the Slab

In terms of optical depth, the penetration is determined by

$$\Delta\tau = l \cos\vartheta_2$$

$$\tau_2 = \tau_1 + \Delta\tau$$

where l is the optical distance, τ_1 and τ_2 are the optical depths for two successive collisions, and $\Delta\tau$ is the increment of optical depth between the two collisions.

The height at which the collision occurs can be calculated from the relation between the optical depth and the height according to atmospheric profile. Suppose the heights for two successive collisions are h_1 and h_2 , the distance traveled between collisions is

$$d = (h_2 - h_1) / \cos\vartheta_2$$

3.2.5. Horizontal Displacement

The horizontal displacement can then be calculated.

$$\Delta x = d \sin\vartheta_2 \cos\varphi_2$$

$$\Delta y = d \sin\vartheta_2 \sin\varphi_2$$

where Δx and Δy are the coordinate increments in S-N and E-W directions, respectively, and the horizontal location x_2, y_2 can be derived given the location before the current travel path x_1, y_1 .

$$x_2 = x_1 + \Delta x$$

$$y_2 = y_1 + \Delta y$$

3.2.6. Escape

If the current accumulative optical depth τ_2 is less than 0, the photon is reflected, and this case can be ignored since the present algorithm only deals with the transmission problem. If τ_2 is greater than the total optical depth of the slab, the photon escapes at the bottom of the slab and contributes to the point-spread function. The horizontal location should be calculated using a modified traveling distance which is shorter than what has been calculated from the random process. The horizontal location thus obtained and the current travel direction should be recorded properly in order to get an accurate description of the point-spread function.

This concept can also be slightly modified using the photon bundle mention before. Suppose a fraction of a photon bundle f_1 travels in direction ϑ, φ starting from τ, x, y . For $\vartheta > \pi/2$, the fraction of the photon bundle f_2 that will escape at the top of the slab is

$$f_2 = f_1 e^{-(\tau/|\cos\vartheta|)}$$

For $0 \leq \vartheta < \pi/2$,

$$f_2 = f_1 e^{-(\tau^* - \tau)/(\cos\vartheta)}$$

For $\vartheta = \pi/2$,

$$f_2 = 0$$

τ^* is the total optical depth. The horizontal position of escaping in the manner described earlier. The remaining portion of the photon bundle $f_1 - f_2$ will still travel within the slab. The distance traveled related to random number τ_1 can be determined from

$$l = |\ln(1 - \tau_1 (1 - \frac{f_2}{f_1}))|$$

Such a process along with the absorption process upon collision for non-conservative scattering makes the remaining portion of the photon bundle smaller and smaller and eventually the remaining fraction is so small that it can be neglected. Such a treatment can save computation time for given precision.

3.2.7. Discretization of Angles and Distance

When the photon travels within the slab, the locations of the photon are calculated in a continuous manner so that no error is accumulated. However, at the point the photon escapes at the bottom of the slab, we have to record the escaping location and direction of the photon in a discrete manner. Four dimensions of discretization may be applied since the distribution of the escaping photon is a function of location coordinates of x, y and angular coordinates ϑ, φ . An array of 4 dimensions takes a lot of computer memory space, and to make the recorded photon number in each element of such an array statistically meaningful, the total number of photons needed in the experiment must be tremendously large. Therefore such an algorithm is infeasible. Under the assumption that the photon impinges at the top of the slab perpendicularly, the point-spread function is axisymmetric and we need to record the information along a single radius only instead of over the entire x, y plane. Therefore a recording array of only 3 dimensions is needed. We fix the single recording radius along the x axis and put on it the results from the location away from it by rotation. The rotation angle φ_r is

$$\tan\varphi_r = y_2/x_2$$

Note that the signs of x_2 and y_2 allow φ_r to be determined over the range 0 to 2π . After rotation, the zenith angle remains the same while the azimuth angle is changed. Therefore the new zenith angle ϑ is

$$\vartheta = \vartheta_2$$

and the new azimuth angle φ is

$$\varphi = \varphi_2 - \varphi_r$$

The distance of the total horizontal displacement is

$$r = \sqrt{x_2^2 + y_2^2}$$

Later on we will see that for a Lambertian surface, the discretization of ϑ and φ are not necessary, only the spatial discretization is needed. For such a case, the computer resources needed can be reduced, and the non-axisymmetric case would be computationally possible.

ORIGINAL PAGE IS
OF POOR QUALITY

For the axisymmetric case, the discretizations of τ , ϑ , and φ can be performed in the following manner:

For the τ -dimension, an equal increment discretization scheme is carried out. The increment of τ should be equal to or less than the ground resolution of the pixel. For zenith angle ϑ -dimension, the double Gaussian quadrature rule for cosine of zenith angle is the suitable one because the result obtained will be comparable to those produced in the layer adding radiative transfer model. For the azimuth angle domain, the best discretization is the equal increment scheme. The range covered by each element can be determined by finding the midpoints between the adjacent discrete points.

3.2.8. Calculation of the Point Spread Function

In digital image processing, we need to express the point-spread function (*PSF*) in matrix format. If we superimpose such a matrix over a matrix whose elements represent surface irradiance, then the product of two corresponding elements in these two matrices represents the contribution made by the irradiance from that particular ground element to the radiance measured by the satellite, and the sum of the products within the *PSF* window is the total contribution made by ground radiation to the signature of the pixel that coincides with the central element of the *PSF* matrix.

In order to construct such a matrix, we need some corrections to the results obtained directly from the Monte Carlo method.

First is the correction for the difference between areas covered for a fixed increment of radius Δr but for different values of radius r . This is obvious, since the central point's influence ranges from 0 to $\frac{1}{2}\Delta r$ and therefore the influence area is $(\pi/4) \Delta r^2$. Other points' influences range from $r - \frac{1}{2}\Delta r$ to $r + \frac{1}{2}\Delta r$ with area $2\pi r \Delta r$. Therefore it is necessary to make the area correction to get the contribution per unit area.

Secondly, the difference between the area of a circle and the area of square or rectangle must be corrected. For a matrix, the most convenient shape for each element is square or rectangle.

After these corrections, the contribution made by the surface radiation from a unit area of Lambertian surface for the central ground element and the surrounding elements can be expressed as

$$w_0 = \frac{\sum_{\varphi} \sum_{\vartheta} N(\tau_0, \vartheta, \varphi) C}{N_T}$$

$$w_r = \frac{\sum_{\varphi} \sum_{\vartheta} N(r, \vartheta, \varphi) C}{N_T \frac{8r}{\Delta r}}$$

w_0 is the central element of the matrix of the point-spread function, and w_r is an element other than the central one with distance from center r . N is the 3-dimensional array obtained in the Monte Carlo algorithm, and N_T is the total number of photons incident at the top of the atmospheric slab in the experiment. C corrects for the difference between the area of a circle and that of a square or rectangle. For a square, $C = 4/\pi$. From these equations, it is obvious that only the radius dimension is necessary for Lambertian surface.

The convolution of such a point-spread function matrix with the matrix of ground radiance, in which each ground element is Lambertian, gives the total contribution of surface upwelling radiation field to the satellite measurement, and the satellite measured radiance can be expressed as

$$L^-(\tau_0, \vartheta_0, \varphi_0, \xi_k, \eta_i) = L_{atm}(\tau_0, \vartheta_0, \varphi_0)$$

$$+ \sum_{i=0}^N \sum_{j=0}^N h(x_{k-i}, y_{l-j}) L^-(\tau_g, \vartheta_v, \varphi_v, x_i, y_j)$$

h is the point-spread function matrix of size $M \times M$; it is convolved with a ground matrix of size $N \times N$. The elements of h outside the $M \times M$ window size are all zero. The last term on the right hand side is the convolution term.

The point-spread function matrix thus defined only works for the isotropic surface. For anisotropic surface, we need to define the contribution factors for the central ground element and the surrounding elements, respectively.

$$\begin{aligned} A_0 &= \frac{\sum_{\varphi} \sum_{\vartheta} L^-(\tau_g, \vartheta, \varphi, x_0, y_0) N(\tau_0, \vartheta, \varphi) C}{M(\tau_g, x_0, y_0) N_T} \\ &= \frac{C}{\pi N_T} \sum_{\varphi} \sum_{\vartheta} ETA(\tau_g, \vartheta, \varphi, x_0, y_0) N(\tau_0, \vartheta, \varphi) \\ A_{ij} &= \frac{\sum_{\varphi} \sum_{\vartheta} L^-(\tau_g, \vartheta, \varphi, x_i, y_j) N(\tau_{ij}, \vartheta, \varphi) C \Delta r}{8 M(\tau_g, x_i, y_j) \tau_{ij} N_T} \\ &= \frac{C \Delta r}{8 \pi \tau_{ij} N_T} \sum_{\varphi} \sum_{\vartheta} ETA(\tau_g, \vartheta, \varphi, x_i, y_j) N(\tau_{ij}, \vartheta, \varphi) \end{aligned}$$

ETA is the anisotropic factor for upwelling radiation under given illumination condition, and is defined as

$$ETA(\tau_g, \vartheta, \varphi, x, y) = \frac{\pi L^-(\tau_g, \vartheta, \varphi, x, y)}{M(\tau_g, x, y)}$$

M is the exitance at given location. Then the satellite measurement of the radiance is

$$\begin{aligned} L^-(\tau_0, \vartheta_v, \varphi_v, \xi_k, \eta_l) &= L_{atm}^-(\tau_0, \vartheta_v, \varphi_v) \\ &+ \sum_{i=0}^N \sum_{j=0}^N h_A(x_{k-i}, y_{l-j}) M(\tau_g, x_i, y_j) \end{aligned}$$

h_A is the element of the matrix composed of the contribution A_{ij} 's. For a Lambertian surface, a simpler formula can be used.

$$\begin{aligned} L^-(\tau_0, \vartheta_v, \varphi_v, \xi_k, \eta_l) &= L_{atm}^-(\tau_0, \vartheta_v, \varphi_v) \\ &+ \sum_{i=0}^N \sum_{j=0}^N h(x_{k-i}, y_{l-j}) L^-(\tau_g, x_i, y_j) \end{aligned}$$

h is the element of the matrix composed of weight w_0 and w_r 's.

From these equations, it is obvious that if the point-spread function is derived from the Monte Carlo method and if the surface exitance and the pattern of the radiance angular distribution at each surface location are known, the vertically upwelling radiance at satellite level can be determined.

This is the forward aspect of our problem. However, in remote sensing, the reverse aspect of the problem is of more significance, but it is more difficult, too. In the following section, we discuss the inverse problem.

3.3. Retrieval of the Surface Exitance

After removing the atmospheric reflection and source term L_{atm} from the satellite measurement, we have an image g . Also, we can construct a matrix H from the point-spread function such that the size of H is comparable to the lexicographic form, by which the rows of a matrix are stacked to form a vector of the matrix g , and the lexicographic form of the corresponding matrix of surface exitance f . The relationship between f , g , and H is

$$g = H f$$

If there is no noise other than the atmospheric effect, then the surface exitance can be retrieved by the inverse filter given g .

$$f = H^{-1} g$$

The Fourier transform technique can reduce the computation time for the inverse filtering [Andrews and Hunt, 1977]. In the presence of noise, other types of filters may be employed using the point-spread function along with some *a priori* knowledge of noise [Andrews and Hunt, 1977]. However, those procedures are more complicated and the extent to which the result can be improved strongly depends on the signal/noise ratio. The Fourier transform technique similar to that used in inverse filtering can also be used in those filters, to reduce computation time.

REFERENCES

- Andrews, H.C., and B.R. Hunt, 1977, *Digital Image Restoration*, Prentice-Hall, New Jersey.
- Barnes, J.C., and C.J. Bowley, 1974. Handbook of techniques for satellite snow mapping. NASA/GSFC, Final Report, NAS 5-21803, 95 pp.
- Brown, A.J., J.F. Hannaford, and R.L. Hall, 1980. Application of snowcovered area to runoff forecasting in selected basins of the Sierra Nevada, California. In *Operational Applications of Satellite Snowcover Observations*, NASA Pub. 2116, pp. 185-201.
- Cashwell, E.D., and C.J. Everett, 1959, *A Practical Manual of the Monte Carlo Method for Random Walk Problems*, Pergamon Press, New York.
- Chandrasekhar, S., 1960, *Radiative Transfer*, Dover, New York.
- Clark, B. P. and R. Dasgupta, 1983. Landsat-4 Multispectral Scanner (MSS) subsystem radiometric characterization. NASA/GSFC 435-D-404.
- Deutsch, M., D.R. Wiesnet, and A. Rango, Eds., 1981. *Satellite Hydrology*. American Water Resources Association, 730 pp.
- Dozier, J., 1980a. A clear-sky spectral solar radiation model for snow-covered mountainous terrain. *Water Resources Research*, 16, 709-718.
- Dozier, J., 1980b. Improved algorithm for calculation of UTM and geodetic coordinates. *NOAA Technical Report NESS 81*.
- Dozier, J., 1981. A method for satellite identification of surface temperature fields of subpixel resolution. *Remote Sensing of Environment*, 11, 221-229.
- Dozier, J., 1982. Remote sensing of the snow surface radiation budget. *Invited paper*: presented at fall meeting of AGU, San Francisco, CA, H21A-06.
- Dozier, J., 1983. Snow reflectance from Thematic Mapper. In: *Proceedings of Landsat-4 Investigators Early Results Symposium*, NASA, GSFC, in press.

- Dozier, J., J. Frew, and D. Marks, 1980. The use of environmental satellite data for input to energy balance snowmelt models. Final Report, *NOAA Grant 04-8-MO*.
- Dozier, J., and J. Frew, 1981. Atmospheric corrections to satellite radiometric data over rugged terrain. *Remote Sensing of Environment*, 11, 191-205.
- Dozier, J., S.R. Schneider, and D.F. McGinnis, Jr., 1981. Effect of grain size and snowpack water equivalence on visible and near-infrared satellite observations of snow. *Water Resources Research*, 17, 1213-1221.
- Dozier, J., and S.G. Warren, 1982. Effect of viewing angle on the infrared brightness temperature of snow. *Water Resources Research*, 18, 1424-1434.
- Engel, J. L., 1980. Thematic Mapper - an interim report of anticipated performance. in: *Applications notice for participation in the Landsat-D image data quality analysis program*. NASA/GSFC, October 23, 1981.
- Foster, J.L., and A. Rango, 1975. A method for improving the location of the snowline in forested areas using satellite imagery. *NASA/GSFC Pub. X-910-75-41*, 8 pp.
- Frampton, M.J., and D. Marks, 1980. Mapping surface temperature from thermal satellite data in the southern Sierra Nevada. In *Proceedings of the 1980 Western Snow Conference*, pp 88-90.
- Gordon, H.R., 1978, Removal of atmospheric effects from satellite imagery of the oceans, *Applied Optics*, 17, 1631-1636.
- Gordon, H.R., and D.K. Clark, 1980, Atmospheric effects in remote sensing of phytoplankton pigments, *Boundary-Layer Meteorology*, 18, 299-313.
- Grant, I.P., and G.E. Hunt, 1969, Discrete space theory of radiative transfer, 1, Fundamentals, *Proceedings of the Royal Society of London*, Series A, 313, 183-197.
- Hannaford, J.F., 1977. Investigation application of satellite imagery to hydrologic modeling snowmelt runoff in the southern Sierra Nevada, Phase 1. Final Report, *NASA/GSFC, 5-2207*, 48 pp.
- House, L., and L. Avery, 1969, The Monte-Carlo technique applied to radiative transfer, *Journal of Quantitative Spectroscopy and Radiative Transfer*, 9, 1579-1591.
- Lauritson, L., G.J. Nelson, and F.W. Porto, 1979. Data extraction and calibration of TIROS-N/NOAA radiometers. *NOAA Technical Memorandum NESS 107*.
- Marks, D., 1982. Net all-wave radiation as an index to snowmelt runoff. *Paper*: presented at the fall meeting of the AGU, San Francisco, CA, H31A-07.
- Marks, D., J. Dozier, and J. Frew, 1983. Automated basin delineation from digital terrain data. *NASA Technical Memorandum 84984*, 21 pp.
- Martinec, J., 1975. Snowmelt-runoff model for stream flow forecasts. *Nordic Hydrology*, 6, 145-154.
- McGinnis, D.F., Jr., J.A. Pritchard, and D.R. Wiesnet, 1975. Determination of snow depth and snow extent from NOAA-2 satellite Very High Resolution Radiometer data. *Water Resources Research*, 11, 897-902.
- Pearce, W.A., 1977, A study of the effects of the atmosphere on thematic mapper observations, Report No. 004-77, Contract NO. NAS5-23639, EG&G / Washington Analytical Service Center, Inc., Riverdale, MD.
- Rango, A., 1978. Pilot tests of satellite snowcover/runoff forecasting systems. *NASA Technical Memorandum, 78109*, 13 pp.
- Rango, A., 1979. Remote sensing of snow and ice: A review of research in the United States 1975-1978. *NASA Technical Memorandum 79713*, 31 pp.

- Rango, A., and Salomonson, 1976. Satellite snow observations and seasonal streamflow forecasts. Final Report: *NOAA Contract NA-776-74*, 19 pp.
- Rango, A., and K.I. Itten, 1976. Satellite potentials in snowcover monitoring and runoff prediction. *Nordic Hydrology*, 7, 209-230.
- Rango, A., V. Salomonson, and J.L. Foster, 1977. Seasonal streamflow estimation in the Himalayan region employing meteorological satellite snow cover observations. *Water Resources Research*, 14, 359-373.
- Rango, A., and J. Martinec, 1979. Application of a snowmelt-runoff model using Landsat data. *Nordic Hydrology*, 10, 225-238.
- Rango, A., J.F. Hannaford, R.L. Hall, M. Rosenzweig, A.J. Brown, 1979. Snow covered area utilization in runoff forecasts. *ASCE, Journal of the Hydraulics Division*, 105 (HY1), 53-66.
- Smith, R.C., and W.H. Wilson, 1981. Ship and satellite bio-optical research in the California Bight, in: *Oceanography from Space*, pp. 281-294, Ed. by J.F.R. Gower, New York, Plenum Press.
- Snyder, J.P., 1981. Space Oblique Mercator projection mathematical development. *U.S. Geological Survey Bulletin* 1518.
- Wiscombe, W.J., 1977a, Extension of the doubling method to inhomogeneous sources, *Journal of Quantitative Spectroscopy and Radiative Transfer*, 18, 477-489.
- Wiscombe, W.J., 1978b, On initialization, error and flux conservation in the doubling method, *Journal of Quantitative Spectroscopy and Radiative Transfer*, 18, 637-658.
- Wiscombe, W.J., 1981, Computer code ATRAD80 (unpublished).